Title

Back-to-back optical coherence tomography-ultrasound probe for co-registered three-dimensional intravascular imaging with real-time display

ISBN

9780819498472

Authors

Li, Jiawen
Ma, Teng
Jing, Joseph
et al.

Publication Date

2014-03-04

DOI

10.1117/12.2038270

Back-to-back optical coherence tomography-ultrasound probe for co-registered three-dimensional intravascular imaging with real-time display

Jiawen Li*, Teng Ma*, Joseph Jing, Jun Zhang, Pranav M. Patel, K. Kirk Shung, Qifa Zhou and Zhongping Chen

From the Department of Biomedical Engineering (J.L., J.J., and Z.C.), Division of Cardiology (P.M.P.), Beckman Laser Institute (J.L., J.J., J.Z and Z.C.), The Edwards Lifesciences Center for Advanced Cardiovascular Technology (J.L., P.M.P. and Z.C.), University of California, Irvine, Irvine, CA, 92617; and the NIH Ultrasonic Transducer Resource Center (T.M., K.K.S. and Q.Z.), University of Southern California, Los Angeles, CA 90089
* Co-first authors

ABSTRACT

We have developed a novel integrated optical coherence tomography (OCT)-intravascular ultrasound (IVUS) probe, with a 1.5 mm-long rigid-part and 0.9 mm outer diameter, for real-time intracoronary imaging of atherosclerotic plaques and guiding interventional procedures. By placing the OCT ball lens and IVUS 45MHz single element transducer back-to-back at the same axial position, this probe can provide automatically co-registered, co-axial OCT-IVUS imaging. To demonstrate its capability, 3D OCT-IVUS imaging of a pig's coronary artery in real-time displayed in polar coordinates, as well as images of two major types of advanced plaques in human cadaver coronary segments, was obtained using this probe and our upgraded system. Histology validation is also presented.

Keywords: Vulnerable plaque, intravascular ultrasound, optical coherence tomography, online co-registration

1 INTRODUCTION

Each year, more than 20 million patients with coronary artery disease (CAD) experience acute coronary syndrome (ACS) (1). Thirty-four percent of these individuals die from CAD complications in a given year (2). ACS is caused by the accumulation of vulnerable atherosclerotic plaques within coronary artery walls. Since most CAD occurs at a length scale of 2-2000μm, it is essential to have high-resolution and deep-penetration imaging technology on this scale to resolve vascular plaque elements in the coronary artery wall. Currently, only intravascular ultrasound (IVUS) and intravascular optical coherence tomography (OCT) are able to provide cross-sectional, real-time visualization of the coronary artery wall. However, due to intrinsic limitations of resolution and penetration depth, respectively, neither IVUS nor OCT alone is able to accurately assess plaque characteristics (3-5). Combined use of IVUS and OCT holds the potential of combining the strengths of both imaging modalities and improving the diagnostic accuracy of plaque vulnerability. Thus, fusion of these disparate medical image modalities is clinically important to provide improved diagnostic information.

There have been several reports demonstrating the feasibility and potential effectiveness of the combined use of OCT and IVUS in different clinical settings for plaque characterization (6-8) and thin-cap fibroatheroma (TCFA) recognition (4, 9). Nevertheless, there are major limitations with previous approaches using offline fusion of OCT and IVUS (4-9): prior to fusion, matching OCT and IVUS lesions based on manual identification of landmarks, such as side-branches or calcification, is required. The matching procedures are not only tediously slow but also may lead to inaccurate co-registration, because lumens constantly change shape and images acquired may not be identical at

Optical Coherence Tomography and Coherence Domain Optical Methods in Biomedicine XVIII, edited by Joseph A. Izatt, James G. Fujimoto, Valery V. Tuchin, Proc. of SPIE Vol. 8934, 893428 · © 2014 SPIE · CCC code: 1605-7422/14/$18 · doi: 10.1117/12.2038270

different time points within each cardiac cycle. They cannot be used for real-time display either, severely limiting clinical utility for guiding interventions during a catheterization procedure. The ability to fully integrate OCT and IVUS capabilities into a single imaging system for *in vivo* assessment of plaques (9, 10) will help overcome these limitations. Fully-integrated techniques are also less time consuming, less traumatic, provide less radiation exposure, use fewer contrast agents, and provide more accurate imaging capabilities with the potential for a real-time fusion image display.

In preliminary research, our group first developed an integrated OCT-IVUS system and imaging probe (11-13). Independently, Li et al. (14) designed a similar hybrid OCT-IVUS system and used it for *in vitro* human cadaver imaging. Recently, we reported the safe and successful *in vivo* imaging of plaques in rabbits and coronary arteries in a swine using a miniature probe design (12). For the first time, this study showed that an integrated intracoronary OCT-IVUS system is feasible and safe to use *in vivo* to detect atherosclerotic plaques, attracting more attentions by medical doctors to this promising technology. However, one limitation of the previously employed miniature probe (12) was its difficulty to co-register data in real-time due to the offset between the OCT prism and IVUS transducer. For a steady object, offline processing that shifts two images relative to the separation of the probes can possibly fuse OCT-IVUS images of the same region of interest (ROI). However, for *in vivo* imaging, constant changes in lumen geometry renders co-registering images unreasonable, given there is an offset between OCT and US probes.

In this paper, we present a novel design of a miniature integrated probe that overcomes this limitation. The new design uses back-to-back OCT-IVUS probes to facilitate imaging at the same ROI simultaneously. This catheter enables real-time imaging and display of co-registered OCT/IVUS images for identifying vulnerable plaques and guiding coronary intervention which better fits clinical needs compared to the previous probe design with an offline fusion method. In addition, our most current integrated probe design has an identical rigid-part size with the clinically-used IVUS or OCT probe, has a clinically acceptable outer diameter (OD), and does not sacrifice image quality. The reduction in probe size is essential to enable safer OCT/IVUS delivery for clinical applications. We report the first demonstration of real-time 3D imaging and display of co-registered OCT/IVUS images in polar coordinates. The first 3D intracoronary imaging (15) of familial hypercholesterolemic (FH) swine, a common animal model for atherosclerosis study, is shown herein. Images of two major types of advanced atherosclerotic plaques in human cadaver coronary segments further demonstrate the imaging capability of this novel probe.

2 METHODS

With the guidance of visible light from the OCT-sub probe, a back-to-back, co-registered OCT-IVUS probe (Fig.1) was made by carefully aligning an OCT sub-probe with an IVUS sub-probe while confirming that the light beam and sound wave exit at the same axial position, but 180 degrees apart. This integrated probe provides automatically co-registered and co-axial fusion imaging. The combined probe was then inserted into a customized probe cap (a stainless steel tube with two windows, OD: 0.9 mm, length: 1.5 mm). Following the probe cap, we used a double wrapped torque coil (OD: 0.68 mm) to encompass the fiber and electrical wire, giving the probe adequate flexibility and torque control. During experiments, the probe was inserted into a sheath to avoid cross-contamination between probe and cadaver segments. Water was filled in the sheath to facilitate ultrasound imaging.

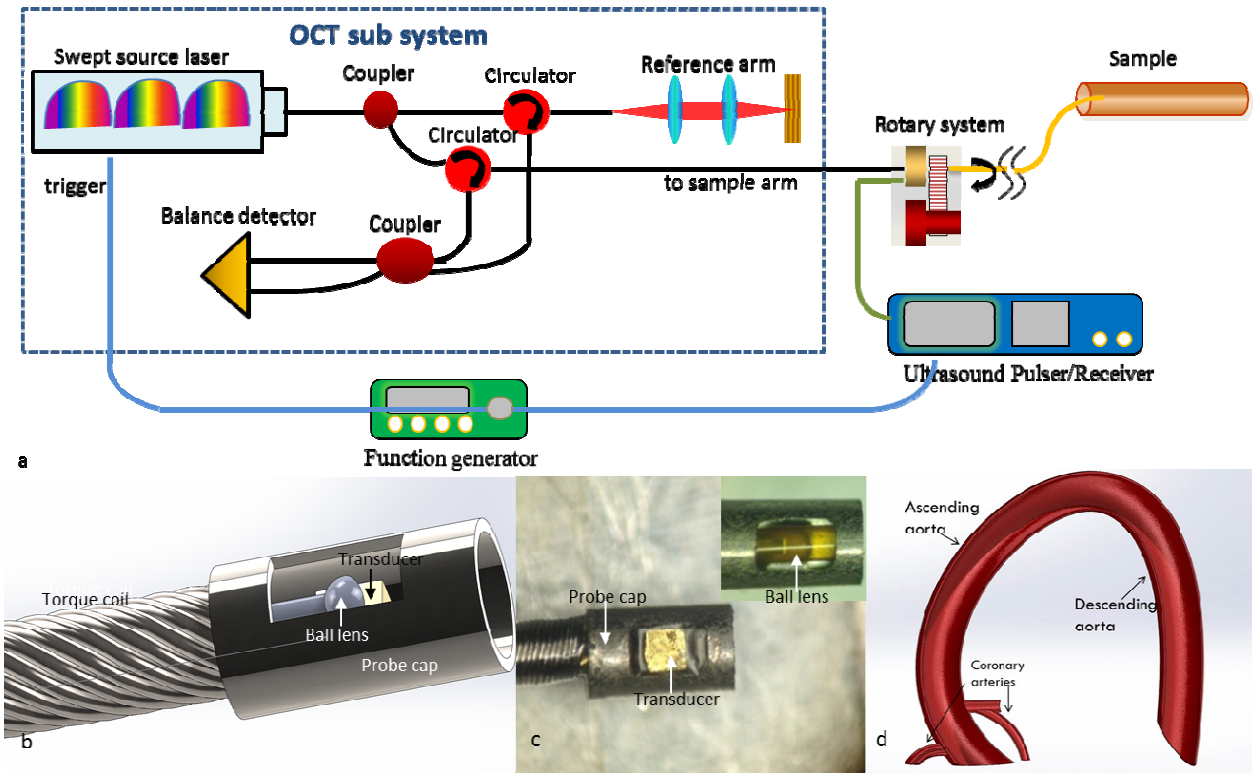

Figure 1. a) Schematic of the integrated imaging system. The dashed box illustrates the OCT sub-system, a swept source OCT system. Black lines, a green line and a blue line denote the optical path, the ultrasound path and the electrical trigger signal, respectively (original schematic published in JACC supplementary information). b) Schematic of back-to-back OCT-IVUS probe. c) Photo of back-to-back probe, showing the transducer. Insert: photo showing the OCT sub-probe. d) Schematic of cardiovascular system.

We used a 0.4 mm x 0.4 mm x 0.3 mm 45 MHz PMN-PT single element transducer for our IVUS sub-probe which is thinner than previous designs (11, 12). The IVUS transducer was fabricated based on the PMN-PT single crystal with a high piezoelectric coefficient (d33=2000pm/V) and electromechanical coupling coefficient (kt=0.58). The PMN-PT plate was lapped to the designed thickness 40µm for 45MHz with 1500 Å chrome/gold (Cr/Au) layers as electrodes coated on both sides. A 10µm matching layer made of a mixture of Insulate 501 epoxy (American Safety Technologies, Roseland, NJ) was cast onto the front side of PMN-PT plates. The conductive backing made of silver epoxy (E-Solder 3022, Von Roll Isola Inc., New Haven, CT) was cast and centrifuged onto the back side of PMN-PT plates. The matched/backed plate was finally lapped to a thickness of only 300µm before mechanically dicing into 0.4mm×0.4mm square shape. The center core of a 46 AWB coaxial cable was connected to the side of the backing layer (back electrode) and covered by epoxy (Epo-Tek 30, Epoxy Technologies, Billerica, MA) to insulate from the front electrode without increasing the thickness of the transducer. The front surface of the matching layer was connected to the metallic shield of the coaxial cable with Cr/Au as the grounding connection. A parylene layer 10µm thick was vapor-deposited on to the transducer to serve as the second matching and waterproof layer. The transducer was carefully glued on to the center of the ball lens with guidance of the visible light before insertion into the cap. The gap between the transducer and cap was filled with epoxy to reinforce stability. Finally, the proximal end of the coaxial cable was connected to a slip ring to enable rotational scan capability.

For the OCT sub-probe, we chose a ball-lens design, which enables less insertion loss and stronger interfaces (16, 17) than the traditional GRIN lens design (14, 18). Ball lenses also have the potential to be manufactured in large quantities while maintaining constant performance. A single mode fiber (SMF-28 Corning Incorporated; cladding OD: 0.125 mm) was fusion-spliced to a fiber spacer (cladding OD: 0.125 mm; reflective index: 1.457; Prime Optical Fiber Corporation) using a splicing workstation (GPX 3400 system, Vytran LLC). Then, a ball with a 560 µm-long fiber spacer (17) was created at the distal end of the fiber spacer using the splicing workstation. This ball lens can

generate a beam focusing at ~1 mm from the ball surface. Next, the lens was mechanically polished until the angle between the polished surface and optical fiber were less than 37 degrees. The ball lens was later inserted into a sealed polyimide tube, isolating the ball lens from the water in the sheath and maintaining an air-fiber interface to ensure that the total internal reflection was generated at the polished surface.

All imaging was performed using the integrated OCT-IVUS system (12) (Fig. 1a) at 1000 pixels per frame, 10 frames per second, 2.5mm/s pull-back speed. Current system speed is limited by the ultrasound sub-system speed. However, it is possible to improve the imaging pull-back speed to 25mm/s (19), the commercial OCT system speed. The co-registered OCT-IVUS polar domain image pairs were displayed in real-time by rotating OCT images 180 degrees to match IVUS images' orientation and converting them from Cartesian coordinates to polar coordinates using a commercial graphics processing unit package. This is the first report of the capability to display real-time OCT-IVUS imaging in polar coordinates.

We used coronary arteries from swine and human cadavers to demonstrate the imaging capabilities of this probe. FH swine is an ideal atherosclerotic animal model for intravascular imaging (15) since lesions formed in FH swine closely mimic advanced human atherosclerosis. Human coronary arteries, which were up to 3 days postmortem and fixed with formalin, were also used for imaging. Plaques were imaged with this OCT-IVUS integrated system in phosphate buffered saline at room temperature. After imaging, each coronary artery segment was sectioned for histology analysis.

3 RESULTS AND DISCUSSION

A typical cardiovascular system is shown in Fig. 1d. The system includes several sharp turns: from the descending aorta to ascending aorta, there is a curve of over 180 degrees. Furthermore, the right (or left) coronary artery and ascending aorta are normally 80-90 degrees angularly spaced. This curvy structure demands a probe with high flexibility, small diameter, and short length of the rigid-part to provide safe access to the coronary arteries. In previously reported probe designs (11-14), either the probe's OD was too large or the rigid-part was too long, both of which potentially reduced the safety of catheter interventions. The probe previously reported by our group has a 0.7 mm OD but a rigid-part as long as ~3.5 mm (12) while the probe reported by Li (14) has a 2.5 mm-long rigid part, but an OD as large as 1.0 mm. The back-to-back ball-lens design probe reported here minimizes the probe's rigid-part to 1.5 mm-long, which is the same size as clinically-used IVUS or OCT rigid-parts, while maintaining an OD of 0.9 mm. The reduction of probe size is a significant improvement which allows for safer access to the coronary artery system. Using available space more efficiently than previous designs, we further reduced probe size without reducing the size of the optical lenses, hence maintaining image quality. Standard pulse-echo testing (Fig. 2) was performed to evaluate the thinner (300 μm) IVUS transducer's performance. The center frequency of the IVUS transducer was found to be 45 MHz, exhibiting a -6dB fractional bandwidth of 40%. Thus, the IVUS transducer demonstrated satisfactory performance compared to those in previously published reports (11, 12).

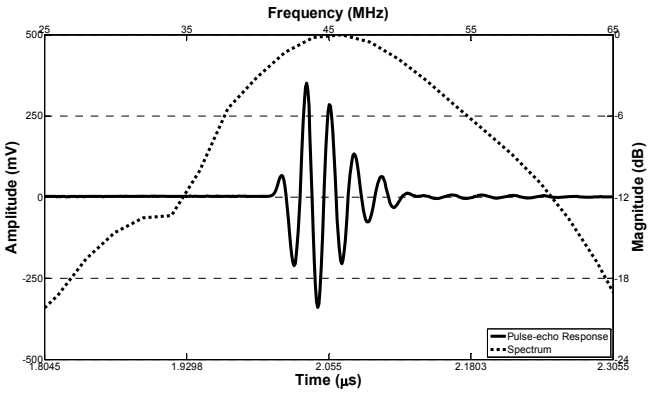

Figure 2. Time domain pulse-echo waveform and frequency spectrum of the IVUS probe with a 1mm-long coaxial cable connecting to a slip ring

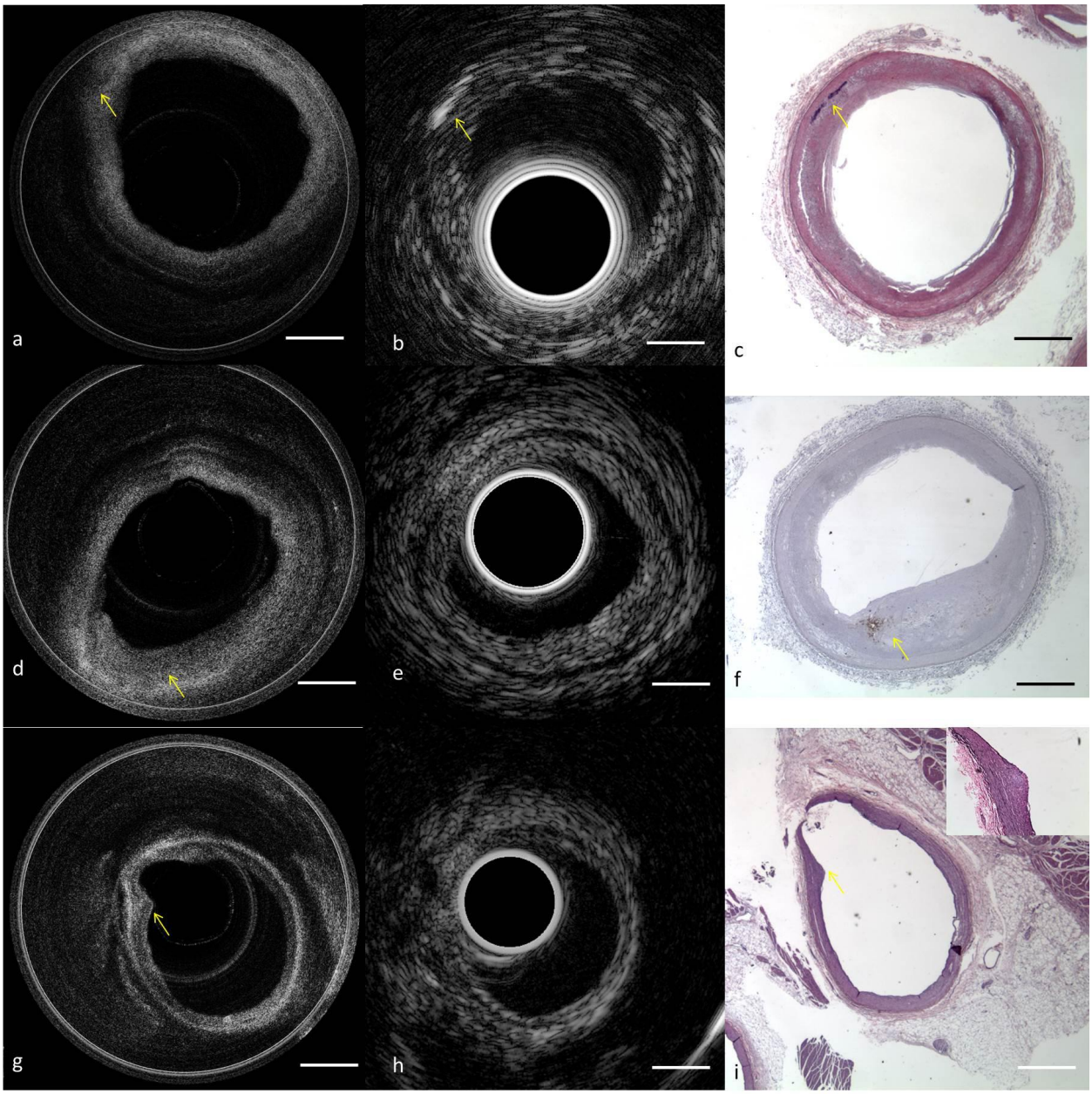

Figure 3. Top row: Images of calcified plaque. (a) OCT and (b) IVUS cross-sectional images of a human coronary artery with calcified plaque; (c) corresponding H&E histology. Middle row: Images of necrotic plaque and fibrous plaque. (d) OCT and (e) IVUS cross-sectional images of a human coronary artery with necrotic plaque and fibrous plaque; (f) corresponding CD68 histology. Bottom row: Images of FH swine coronary artery with early atherosclerotic plaque. (g) OCT and (h) IVUS (i) corresponding H&E histology. Inset: magnified elastic histology.

Representative OCT-IVUS image pairs of coronary artery segments with calcified plaque and necrotic plaque are shown in Fig. 3a-f. Sharp boundaries in OCT (Fig. 3a, arrow) and acoustic shadows in IVUS (Fig. 3b, arrow) demonstrate the locations of calcified plaques. Signal-high regions in OCT (Fig. 3d) demonstrate the locations of fibrous plaques. The signal-low region overlaying the diffused boundary in OCT (Fig. 3d, arrow) demonstrates the location of a necrotic plaque. Histology photos validate the plaque type classification by OCT-IVUS images. We

also scanned a 5 cm-long segment of swine coronary artery to investigate the existence and location of plaques, and to our knowledge, this is the first intravascular imaging of FH swine coronary artery that revealed the existence of atherosclerotic plaques (Fig.3g-i).

4 CONCLUSION

In summary, we have developed a novel miniature probe for automatically co-registered OCT-IVUS imaging. With our probe and system, 3D OCT-IVUS imaging with online real-time fusion is achieved. Real-time 3D imaging of a FH swine coronary artery demonstrated the co-registered nature of this probe and the polar image display capability of this system. Human plaques' morphologic characteristics were also clearly imaged. This design enables real-time *in situ* characterization of plaques and guiding of coronary intervention which is essential in translating this technology from bench to clinical application.

ACKNOWLEDGMENTS

This work was supported by the National Institutes of Health under grants R01EB-10090, R01HL-105215, R01EY-021519, P41-EB002182, P41EB-015890. We acknowledge Ms. Leacky Liaw, Ms. Linda Li, Mr. Hataka Minami and Mr. Andrew Heidari for their assistance in histology and Solidwork drawing. The authors wish to thank individuals who donated their bodies and tissues for the advancement of education and research.

REFERENCES

1. WHO. The world health report 2002 - Reducing Risks, Promoting Healthy Life. 2002.
2. Véronique L. Roger ASG, Donald M. Lloyd-Jones, Robert J. Adams, Jarett D. Berry,Todd M. Brown, Mercedes R. Carnethon, Shifan Dai, Giovanni de Simone, Earl S. Ford, Caroline S. Fox, Heather J. Fullerton, Cathleen Gillespie, Kurt J. Greenlund, Susan M. Hailpern, John A. Heit, P. Michael Ho, Virginia J. Howard, Brett M. Kissela, Steven J. Kittner, Daniel T. Lackland, Judith H. Lichtman, Lynda D. Lisabeth, Diane M. Makuc,Gregory M. Marcus, Ariane Marelli, David B. Matchar, Mary M. McDermott, James B. Meigs, Claudia S. Moy, Dariush Mozaffarian, Michael E. Mussolino, Graham Nichol, Nina P. Paynter, Wayne D. Rosamond, Paul D. Sorlie, Randall S. Stafford, Tanya N. Turan, Melanie B. Turner, Nathan D. Wong, Judith Wylie-Rosett. Heart Disease and Stroke Statistics--2011 Update : A Report From the American heart assoctiation. Circulation. 2011;123:18-209.
3. Troels Thim MKH, David Wallace-Bradley, Juan F. Granada, Greg L. Kaluza, Ludovic Drouet, William P. Paaske, Hans Erik Bøtker, Erling Falk. Unreliable Assessment of Necrotic Core by Virtual Histology Intravascular Ultrasound in Porcine Coronary Artery Disease. Circulation. 2010;3:384-91.
4. Takahiro Sawada JS, Hector M. Garcia-Garcia, Toshiro Shinke,, Satoshi Watanabe HO, Daisuke Matsumoto, Yusuke Tanino,, Daisuke Ogasawara HK, Hiroki Kato, Naoki Miyoshi,, Mitsuhiro Yokoyama PWS, and Ken-ichi Hirata. Feasibility of combined use of intravascular ultrasound radiofrequency data analysis and optical coherence tomography for detecting thin-cap fibroatheroma. European Heart Journal. 2008;29:1136-46.
5. Masanori Kawasaki BEB, Jason Bressner, Stuart L. Houser, , Seemantini K. Nadkarni BDM, Ik-Kyung Jang, Hisayoshi Fujiwara, Guillermo J. Tearney. Diagnostic Accuracy of Optical Coherence Tomography and Integrated Backscatter Intravascular Ultrasound Images for Tissue Characterization of Human Coronary Plaques Journal of the American College of Cardiology. 2006;48(1):81-8.
6. Nieves Gonzalo HMG-G, Evelyn Regar, Peter Barlis, Jolanda Wentzel, Yoshinobu Onuma, Jurgen Ligthart, Patrick W. Serruys. In Vivo Assessment of High-Risk Coronary Plaques at Bifurcations With Combined Intravascular Ultrasound and Optical Coherence Tomography. J Am Coll Cardiol Img. 2009;2(4):473-82.
7. Shigeho Takarada TI, Kohei Ishibashi, Takashi Tanimoto, Kenichi Komukai, Yasushi Ino, Hironori Kitabata, Takashi Kubo, Atsushi Tanaka, Keizo Kimura, Masato Mizukoshi, Takashi Akasaka. The Effect of Lipid and Inflammatory Profiles on the Morphological Changes of Lipid-Rich Plaques in Patients With Non–ST-Segment Elevated Acute Coronary Syndrome Follow-Up Study by Optical Coherence Tomography and Intravascular Ultrasound. J Am Coll Cardiol Intv. 2010;3(7):766-72.

8. Daiji Yoshikawaa HI, Nobutake Kurebayashia, Bummei Satoa, Seiichi Hayakawaa, Hirohiko Andob, Mutsuharu Hayashia, Satoshi Isobea, Takahiro Okumuraa, Akihiro Hirashikia, Kyosuke Takeshitaa, Tetsuya Amanob, Tadayuki Uetanib, Sumio Yamadac, Toyoaki Murohara. Association of cardiorespiratory fitness with

characteristics of coronary plaque: Assessment using integrated backscatter intravascular ultrasound and optical coherence tomography. International Journal of Cardiology. 2013;162(2):123-8.
9. Räber L HJ, Radu MD, Garcia-Garcia HM, Stefanini GG, Moschovitis A, Dijkstra J, Kelbaek H, Windecker S, Serruys PW. Offline fusion of co-registered intravascular ultrasound and frequency domain optical coherence tomography images for the analysis of human atherosclerotic plaques. EuroIntervention. 2012;8(1):98-108.
10. Rishi Puri MIWaSJN. intravascular imaging of vulnerable coronary plaque: current and future concepts. Nature reviews. 2011;8:131-9.
11. Jiechen Yin H-CY, Xiang Li, Jun Zhang, Qifa Zhou, Changhong Hu, K. Kirk Shung, Zhongping Chen. Integrated intravascular optical coherence tomography ultrasound imaging system Journal of biomedical optics. 2010;15(1):010512.
12. Jiechen Yin XL, Joe Jing, Jiawen Li, David Mukai, Sari Mahon, Ahmad Edris, Khiet Hoang, K. Kirk Shung, Matthew Brenner, Jagat Narula,Qifa Zhou, Zhongping Chen. Novel combined miniature optical coherence tomography ultrasound probe for in vivo intravascular imaging. Journal of biomedical optics. 2011;16(6):060505.
13. Xiang Li JY, Changhong Hu, Qifa Zhou, K. Kirk Shung, and Zhongping Chen. High-resolution coregistered intravascular imaging with integrated ultrasound and optical coherence tomography probe. Applied Physics Letters. 2010;97(3):133702.
14. Brian H. Li ASOL, Alan Soong, Chelsea E. Munding, Hyunggyun Lee, Amandeep S. Thind, Nigel R. Munce, Graham A. Wright, Corwyn H. Rowsell, Victor X.D. Yang, Bradley H. Strauss, F. Stuart Foster, Brian K. Courtney. Hybrid intravascular ultrasound and optical coherence tomography catheter for imaging of coronary atherosclerosis. Catheterization and Cardiovascular Interventions. 2012.
15. Damir Hamamdzic RLW. Porcine Models of Accelerated Coronary Atherosclerosis: Role of Diabetes Mellitus and Hypercholesterolemia. Journal of Diabetes Research. 2013;2013:761415.
16. M. Shishkov GJT, and B.E. Bouma. Scultpured optical fiber tips for narrow diameter optical catheters. Biomedical Topical Meeting (BIO) Miami Beach, Florida. 2003.
17. Youxin Mao SC, Costel Flueraru. Fiber lenses for ultra-small probes used in optical coherent tomography. J Biomedical Science and Engineering. 2010;3:27-34.
18. Guillermo J. Tearney MEB, Brett E. Bouma, Stephen A. Boppart, Costas Pitris, James F. Southern and James G. Fujimoto. In Vivo Endoscopic Optical Biopsy with Optical Coherence Tomography. Science. 1997;276:2037-9.
19. Xiang Li, Jiawen Li, Joe Jing, Teng Ma, Shanshan Liang, Jun Zhang, Dilbahar Mohar, Aidan Raney, Sari Mahon, Matthew Brenner, Pranav Patel, K. Kirk Shung, Qifa Zhou, Zhongping Chen. Integrated IVUS-OCT Imaging for Atherosclerotic Plaque Characterization. IEEE Journal of Selected Topics in Quantum Electronics. 2014;20(2):1-8.